J. Fluid Mech. (2006), *vol.* 558, *pp.* 69–78.
doi:10.1017/S0022112006000152 Printed in the United Kingdom

Free convection in laterally solidifying mushy regions

By PETER GUBA† AND M. GRAE WORSTER

Institute of Theoretical Geophysics, Department of Applied Mathematics and Theoretical Physics, University of Cambridge, Wilberforce Road, Cambridge CB3 0WA, UK

(Received 24 June 2004 and in revised form 15 December 2005)

An analysis is presented of the lateral solidification of a semi-infinite mushy region influenced by vertical, buoyancy-driven convection of the residual, interstitial melt. We consider a parameter regime in which the flow is steady on the time scale of the transient evolution of the mushy region. Our idealized model predicts patterns of macrosegregation consistent with earlier experimental studies and sheds light on the mechanisms involved.

1. Introduction

Mushy regions, regions in which liquid and solid phases coexist, are of particular importance in many varied situations, including industrial crystal growth (Hurle 1993), the directional solidification of metallic alloys both in metallurgy (Kurz & Fisher 1989) and the Earth's core (Fearn 1998), and the freezing of silicate magma chambers (Huppert & Sparks 1984). A distillation of the theoretical investigations into the dynamics of mushy regions can be found in recent reviews by Worster (1997, 2000).

Most theoretical studies of convective dynamics in mushy regions have focused on solidification at horizontal boundaries. Yet, as illustrated in a review by Huppert (1990), a wide range of interesting convective behaviours can be observed during the cooling and crystallization of binary alloys from a vertical boundary.

Motivated by geological processes in magma chambers, Turner & Gustafson (1981) performed laboratory experiments in which various aqueous solutions were cooled and solidified from a sidewall in confined spaces. Leitch (1987) and Bloomfield & Huppert (2003) have extended these earlier experiments to investigate, among other issues, the importance of different morphologies of the freezing interface to the evolution of the boundary-layer flows and, in turn, to the structure of the resulting solid. It was observed, for example, that dendritic interfaces act to enhance the rate of crystal growth and development of stratification in the ambient liquid relative to smoother ones.

Previous theoretical studies have considered flow in the liquid external to the solidifying region (e.g. Nilson, McBirney & Baker 1985; Thompson & Szekely 1988; Bloomfield & Huppert 2003). In this paper, we begin a theoretical study of the fundamental properties of coupled solidification and convection within a partially solidified region (mushy region) of a binary solution cooled from the side. We assume

† Present address: Department of Applied Mathematics and Statistics, Faculty of Mathematics, Physics and Informatics, Comenius University, 842 48 Bratislava, Slovakia.

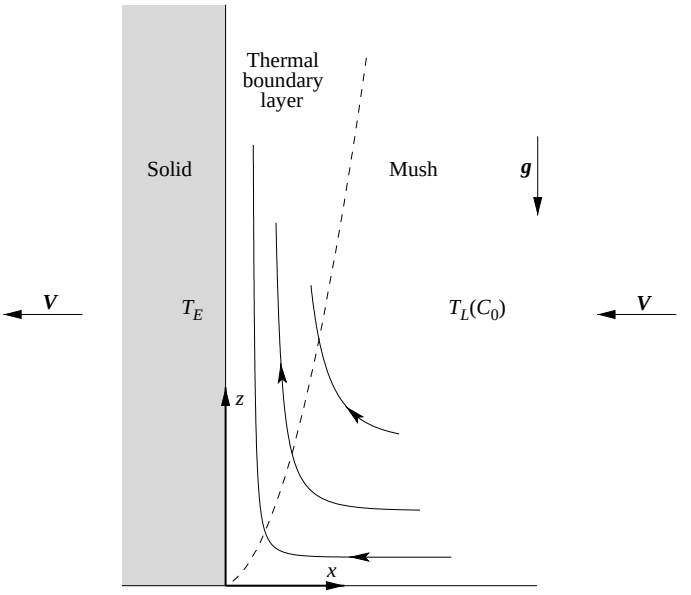

FIGURE 1. Definition sketch. A semi-infinite mushy region of far-field temperature $T_L(C_0)$ solidifies laterally at fixed speed V to form a solid at the eutectic temperature T_E. The release of a buoyant residual is confined to a thermal boundary layer adjacent to the interface. Illustrative streamlines are shown relative to the (moving) solid phase.

that the flow takes place in a narrow thermal boundary layer within the mushy region, which enables substantial simplification of the underlying governing equations. Self-similar solutions of the laminar boundary-layer flows are used to determine many of the important features analytically, and to identify clearly the essential physical mechanisms involved.

In § 2 we describe the model and set out in dimensionless form the equations governing the mushy region during the lateral solidification of a binary alloy. In § 3 we perform a boundary-layer analysis and identify a particular limit that preserves important interactions between convection and solidification. The equations admit a self-similar solution which is presented and discussed in § 4. Finally, in § 5, we give some concluding remarks and discuss the relationship between our results and previous experimental studies.

2. Formulation

We consider a binary alloy that releases a buoyant residual fluid as it solidifies, being pulled horizontally at constant speed V past a heat exchanger that maintains the eutectic temperature T_E (below which the binary system is completely solid) at the fixed vertical plane $x = 0$. The material supplied at $x = \infty$ has the solute composition C_0 and temperature equal to its liquidus temperature $T_L(C_0)$. A mushy region fills the semi-infinite region $x > 0$, $z > 0$, where z is measured vertically upwards (figure 1).

Throughout the mushy region, the temperature and composition are required to satisfy the linear liquidus relationship

$$T = T_L(C) \equiv T_L(C_0) + \Gamma(C - C_0), \tag{2.1}$$

where the liquidus slope Γ is positive. This constraint denies the possibility of the sort of bi-directional convection that can be found in the melt external to solidifying regions (e.g. Nilson *et al.* 1985).

We treat the mushy region as being *ideal* (for a definition, see Worster 1997). The unsteady dimensionless equations governing the mushy region are

$$\left(\frac{\partial}{\partial t}-\frac{\partial}{\partial x}\right)\theta+\boldsymbol{u}\cdot\nabla\theta=\nabla^2\theta+\mathscr{S}\left(\frac{\partial}{\partial t}-\frac{\partial}{\partial x}\right)\phi, \tag{2.2a}$$

$$\left(\frac{\partial}{\partial t}-\frac{\partial}{\partial x}\right)[(1-\phi)\theta+\mathscr{C}\phi]+\boldsymbol{u}\cdot\nabla\theta=0, \tag{2.2b}$$

$$\nabla^2\psi-\frac{1}{\Pi}\nabla\psi\cdot\nabla\Pi=-Ra\Pi\frac{\partial\theta}{\partial x}, \tag{2.2c}$$

where t is dimensionless time, θ is the dimensionless temperature (or composition) defined by $\theta=[T-T_L(C_0)]/\Delta T=(C-C_0)/\Delta C$ with $\Delta C=C_0-C_E$, $\Delta T=\Gamma\Delta C$ and C_E denoting the eutectic concentration, ϕ is the local solid fraction, $\boldsymbol{u}$ is the volume flux (or Darcy velocity), ψ is the stream function defined by $\boldsymbol{u}=(-\psi_z,\psi_x)$, and Π is the permeability. Equations (2.2) have been rendered dimensionless by scaling velocities with V, lengths and time with κ/V and κ/V^2, respectively, with κ being the thermal diffusivity, and permeability with a reference value Π_0. In general the dimensionless permeability Π is a function of ϕ; for analytical expediency, we shall restrict the mushy region to be of uniform permeability by setting $\Pi=1$. Note that the derivative $\partial/\partial x$ in (2.2*a*, *b*) reflects the rate at which the material is continually being pulled in the horizontal direction (cf. Worster 1997).

The dimensionless groups are the Stefan number, a compositional ratio and a mush Rayleigh number defined respectively by

$$\mathscr{S}=L/(c_p\Delta T),\quad \mathscr{C}=(C_s-C_0)/\Delta C,\quad Ra=\beta\Delta C g\Pi_0/(\nu V), \tag{2.3a–c}$$

where L is the specific latent heat, c_p is the specific heat capacity, C_s is the composition of the solid phase, $\beta=\beta^*-\Gamma\alpha^*$, α^* and β^* being the thermal and solutal expansion coefficients, g is the acceleration due to gravity and ν is the liquid kinematic viscosity. Note that the Rayleigh number is inversely proportional to the solidification rate, so that large values of Ra, which we shall consider shortly, can be achieved by pulling the mush at correspondingly small rates.

In the analysis below, we consider a particular asymptotic regime in which the thermal and flow fields are steady, whilst some transient solidification can still occur. The boundary conditions on the flow and thermal fields are

$$\theta=-1,\quad \psi=0\quad \text{at}\quad x=0\qquad (z>0), \tag{2.4a, b}$$

$$\theta\to 0,\quad \partial\psi/\partial x\to 0\quad \text{as}\quad x\to\infty\quad (z>0). \tag{2.5a, b}$$

The far-field and initial conditions on the local solid fraction are provided in § 4.

3. Boundary-layer equations

We wish to examine the free convective flow, coupled with solidification, at high Rayleigh numbers. In this limit, the flow is confined to a narrow region adjacent to the solid–mush interface. Further, we consider the asymptotic limit of large $\mathscr{C}$ in order that ϕ is kept less than unity throughout most of the domain, and large $\mathscr{S}$ in order to retain the influence of local phase change. These parameter limits are appropriate for systems in which the latent heat released during the solidification is comparable

to the heat associated with the depression of the liquidus. Typical laboratory values (for example in experiments using aqueous solutions) are $Ra \approx 10^3$, $\mathscr{S} \approx 10$, $\mathscr{C} \approx 10$, the latter being achieved by having an initial concentration close to the liquidus.

A scaling analysis of (2.2) suggests the rescalings

$$\mathscr{S} = Ra^{1/2}\bar{\mathscr{S}}, \quad \mathscr{C} = Ra^{1/2}\bar{\mathscr{C}}, \tag{3.1a,b}$$

$$x = Ra^{-1/2}X, \quad t = Ra^{-1/2}T, \quad \psi = Ra^{1/2}\Psi, \tag{3.2a–c}$$

with $\bar{\mathscr{S}}$, $\bar{\mathscr{C}}$, X, T and Ψ assumed $O(1)$ as $Ra \to \infty$. The scalings of x and ψ are typical of vertical, free-convection boundary-layer flows in porous media (e.g. Cheng & Minkowycz 1977; Ingham & Brown 1986), while the scaling of t ensures that some temporal development of the solid fraction can be examined (§4). The particular choice of scalings embodied in (3.1) ensures that all the important interactions between flow, heat and mass transfer and phase change are retained at leading order.

Substituting into (2.2), taking the limit $Ra \to \infty$ and rearranging, we obtain

$$\Omega\left(-\frac{\partial\Psi}{\partial z}\frac{\partial\theta}{\partial X} + \frac{\partial\Psi}{\partial X}\frac{\partial\theta}{\partial z}\right) = \frac{\partial^2\theta}{\partial X^2}, \tag{3.3a}$$

$$\frac{\partial\phi}{\partial T} - \frac{\partial\phi}{\partial X} = -\frac{1}{\Omega\bar{\mathscr{C}}}\frac{\partial^2\theta}{\partial X^2}, \tag{3.3b}$$

$$\frac{\partial^2\Psi}{\partial X^2} = -\frac{\partial\theta}{\partial X}, \tag{3.3c}$$

where $\Omega = 1 + \bar{\mathscr{S}}/\bar{\mathscr{C}}$.

The modified solute-conservation equation (3.3b) deserves some discussion. First, it decouples from the heat balance (3.3a) and the momentum balance (3.3c); this fact hinges on the assumption (3.1b) (the near-eutectic limit, cf. Emms & Fowler 1994). Further, noting that $\Omega = O(1)$, (3.3b) implies that ϕ remains $O(1)$ within the boundary layer. Finally, the solid fraction evolves solely in response to the thermal field; this feature appears characteristic of free mush convection, and is discussed further in §4.

4. Similarity solution

4.1. *Steady solution*

We observe that (3.3a) and (3.3c), subject to (2.4) and (2.5), govern steady-state thermal and flow fields. Note that there is a fast initial phase, $t = O(Ra^{-1})$, during which these fields evolve to their steady states, which we ignore.

We seek a similarity solution of the form

$$\Psi = z^{1/2}f(\eta)/\Omega^{1/2}, \quad \theta = \theta(\eta), \quad \text{where} \quad \eta = \Omega^{1/2}X/z^{1/2}. \tag{4.1a–c}$$

Then, from (3.3c) and (2.5), θ is given by

$$\theta = -f', \tag{4.2}$$

and, from (3.3a), (2.4) and (2.5b), f satisfies

$$f''' + \tfrac{1}{2}ff'' = 0, \tag{4.3}$$

$$f = 0, \quad f' = 1 \quad (\eta = 0); \quad f' \to 0 \quad (\eta \to \infty). \tag{4.4a–c}$$

Equations (4.2)–(4.4) are equivalent to those derived by Cheng & Minkowycz (1977). Thus the flow and thermal fields are qualitatively similar to those in the problem

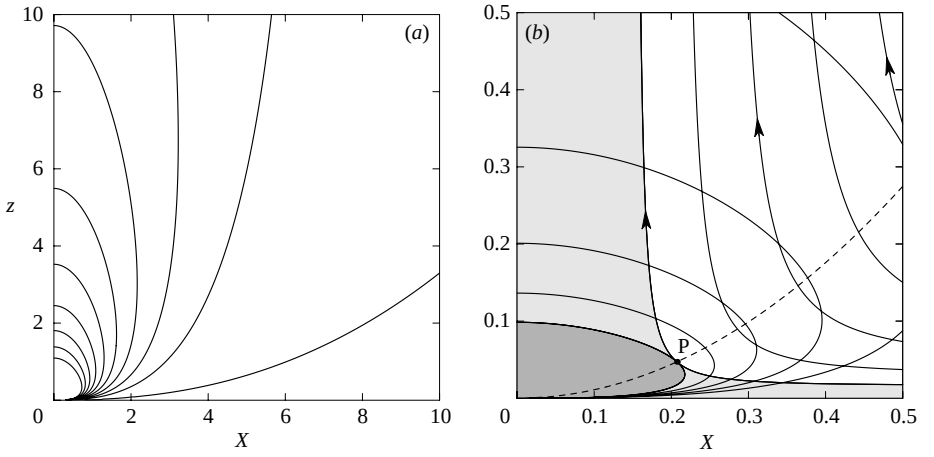

FIGURE 2. (*a*) Contours of the steady-state solid fraction for $\bar{\mathscr{S}} = \bar{\mathscr{C}} = 1$. Contours range from 0.001 to 0.3 by constant increments, starting from the right. (*b*) An enlargement of the region in the vicinity of the leading edge of the interface. Contours of ϕ (solid curves) are shown together with streamlines of $\boldsymbol{u}$ (solid curves with arrows). Contours range from $\phi = 0.4$ to 1 and $\Psi = 0.375$ to 0.149, starting from the right. The dark shading indicates the region where the mush freezes completely, forming a solid inclusion. The light shading indicates the portions in which, in turn, the present theory breaks down; these portions are bounded by a streamline traversing the point P. Also shown is a representative isotherm $\theta = -0.471$ (dashed curve).

without solidification, with quantitative deviations given by the incorporation of Ω in (4.1*a*, *c*).

The rate of heat transfer across the interface is measured by the local Nusselt number, which is given by

$$Nu = \left.\frac{\partial\theta}{\partial x}\right|_{x=0} = Ra^{1/2}\Omega^{1/2}\frac{1}{z^{1/2}}\left.\frac{\mathrm{d}\theta}{\mathrm{d}\eta}\right|_{\eta=0} \approx 0.444 Ra^{1/2}\Omega^{1/2}z^{-1/2}. \tag{4.5}$$

Here the value of $\mathrm{d}\theta/\mathrm{d}\eta|_{\eta=0}$ has been determined from the numerical solution to (4.3) and (4.4). An approximate analytical solution, discussed in the Appendix, provides an estimate $(\frac{3}{28} + \frac{1}{14}(\frac{5}{3})^{1/2})^{1/2} \approx 0.446$. Expression (4.5) shows that the solidification makes the heat transfer more efficient: as Ω rises from unity, the release of latent heat tends to warm the mush, thereby thinning the boundary layer and enhancing the heat transfer out of the mush. The same trend was observed in the experiments by Bloomfield & Huppert (2003); cf. their figure 17.

To find a steady solution to (3.3*b*), the far-field solid fraction, $\phi_\infty(z) \equiv \lim_{X\to\infty}\phi$, must be specified. A similarity solution is admitted provided

$$\phi_\infty(z) = \bar{\phi}_\infty/z^{1/2} \quad (z \geqslant \bar{\phi}_\infty^2), \tag{4.6}$$

where $\bar{\phi}_\infty$ is a prescribed non-negative constant. We choose $\bar{\phi}_\infty = 0$ for simplicity, and integrate (3.3*b*) to obtain

$$\phi(X, z) = \frac{1}{\Omega^{1/2}\bar{\mathscr{C}}}\frac{1}{z^{1/2}}\frac{\mathrm{d}\theta}{\mathrm{d}\eta}. \tag{4.7}$$

This solution is shown in figure 2 for $\bar{\mathscr{S}} = \bar{\mathscr{C}} = 1$. Near the leading edge of the interface, the lateral heat transfer is much higher than in the distal regions up- and downstream, which acts to enhance the local freezing; this is exhibited in figure 2(*a*)

by a bulbous region of increased ϕ close to the edge of the interface. We find that there is a finite region in which complete solidification occurs (figure 2*b*), arising from a singularity in the temperature gradient owing to a discontinuity in boundary conditions on the interface as $z \to 0$. The occurrence of this solid inclusion places further bounds on the validity of our solutions, since in practice the flow cannot pass through it. The region of invalidity is bounded by a limiting streamline that passes through

$$(X_P, z_P) = (\eta_P \Omega^{-1/2} z_P^{1/2}, z_P), \quad \text{with} \quad \eta_P \approx 1.373, \quad z_P \approx 0.093 \Omega^{-1} \bar{\mathscr{C}}^{-2}. \tag{4.8}$$

Since $(X_P, z_P) \propto (\Omega^{-1}\bar{\mathscr{C}}^{-1}, \Omega^{-1}\bar{\mathscr{C}}^{-2})$ the inclusion shrinks self-similarly as either $\bar{\mathscr{S}}$ or $\bar{\mathscr{C}}$ increases, increasing the spatial range for the validity of the model.

Strictly speaking the region where our model is invalid extends all the way up the eutectic front since the streamlines closest to the front have passed through the small corner region of zero porosity. Discounting this region would seem therefore to introduce a global error. However, the temperature and bulk-composition fields are little affected by these few streamlines and our solutions provide good (asymptotic) approximations away from the corner itself. We assess this by examining its relative contribution to the heat budget, which, in terms of the approximate solution (see the Appendix), can be expressed as

$$1 + \theta_\Psi(z) = (b/a - 1)[\exp(a\Psi_P / z^{1/2}) - 1], \tag{4.9}$$

where $\theta_\Psi(z)$ is the temperature along the limiting streamline, $\Psi_P \approx 0.299 \Omega^{-1/2} \bar{\mathscr{C}}^{-1}$ is the corresponding value of the stream function, $a \approx 0.390$ and $b \approx 0.836$. It follows that the buoyancy supply provided by this region decays exponentially along the direction of the free stream, being of relatively minor significance for $z \gtrsim a^2 \Psi_P^2 \approx 0.014 \Omega^{-1} \bar{\mathscr{C}}^{-2}$. Physically, the region of invalidity acts simply to displace the apparent position of the eutectic front. Since there would be restricted flow in this region, the bulk-composition field must be essentially unaltered in that region from what it is just outside.

As the eutectic interface advances into the mushy region, the remaining liquid is solidified, producing a matrix of composite solid around the pure dendritic crystals. Defining a bulk composition in the mush as $\Theta = (1 - \phi)\theta + \mathscr{C}\phi$, we find that the net composition in the eutectic solid depends on the solid fraction at the mush side of the interface, yielding

$$\Theta_i(z) = -1 + \frac{Ra^{1/2}(1 + \mathscr{C})}{[\mathscr{C}(\mathscr{S} + \mathscr{C})]^{1/2}} \left.\frac{\mathrm{d}\theta}{\mathrm{d}\eta}\right|_{\eta=0} \frac{1}{z^{1/2}}. \tag{4.10}$$

This solution is valid for $z \geqslant (\mathrm{d}\theta/\mathrm{d}\eta|_{\eta=0})^2 \Omega^{-1} \bar{\mathscr{C}}^{-2} \approx 0.197 \Omega^{-1} \bar{\mathscr{C}}^{-2}$, the lower bound corresponding to where the edge of the solid inclusion meets the interface and thus where $\Theta = \mathscr{C}$. Note that the remaining liquid at the eutectic boundary makes a contribution of $C_E[1 - \phi(0^+, z)]/C_s$ to the solid fraction already present, i.e. $\phi(0^+, z)$. From (4.10) it follows that the solute content in the eutectic solid decreases with height as $z^{-1/2}$. This qualitative result compares well with the laboratory measurements by Huppert *et al.* (1987).

Another important aspect of the relationship (4.10) is the appearance of a maximum extent of convective solute redistribution,

$$z_{max}/Ra = \frac{(1 + \mathscr{C})^2}{\mathscr{C}(\mathscr{S} + \mathscr{C})} \left(\left.\frac{\mathrm{d}\theta}{\mathrm{d}\eta}\right|_{\eta=0} \right)^2 \approx 0.197 \frac{(1 + \mathscr{C})^2}{\mathscr{C}(\mathscr{S} + \mathscr{C})}, \tag{4.11}$$

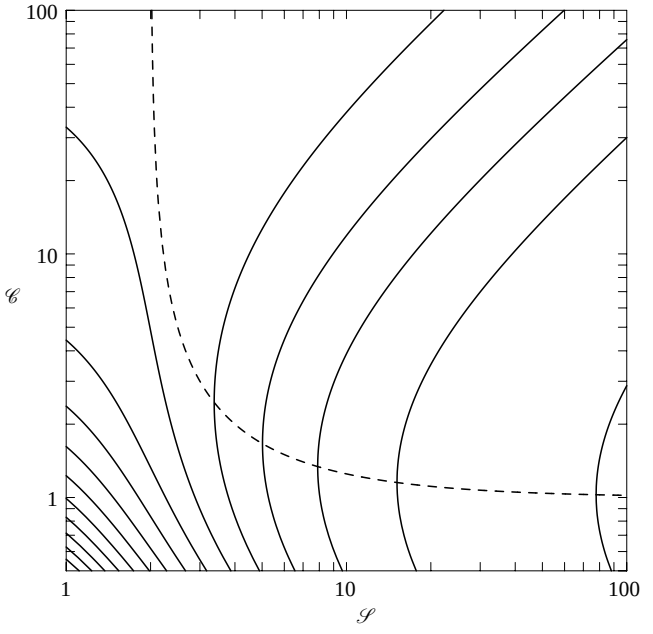

FIGURE 3. Contours of the scaled maximum extent of solute redistribution at the solid–mush interface in the steady state, z_{max}/Ra, as a function of $\mathscr{S}$ and $\mathscr{C}$. Contours range from 0.01 to 0.55 by constant increments, starting from the right. The path of the local minimum of z_{max}/Ra when $\mathscr{C}$ is varied independently of $\mathscr{S}$ is shown dashed.

as can be deduced from (4.10) on setting $\Theta_i = 0$. This allows an insight into the parametric dependences of macrosegregation in the system. Contours of z_{max}, scaled with Ra, as a function of $\mathscr{S}$ and $\mathscr{C}$ are shown in figure 3. At a fixed $\mathscr{C}$, z_{max} decreases monotonically with increasing $\mathscr{S}$. Further, if $\mathscr{C} > \mathscr{S}/(\mathscr{S}-2)$ and $\mathscr{S} > 2$, corresponding to the region above the dashed curve in figure 3, then z_{max} increases as $\mathscr{C}$ increases for a given $\mathscr{S}$. Both behaviours can be understood by considering a flux of solute-depleted fluid at height z in the mush. The latter has the form

$$\mathscr{F}/Ra^{1/2} = -\int_0^\infty W\theta \,\mathrm{d}X = \frac{1}{\Omega^{1/2}} z^{1/2} \int_0^\infty \theta(\eta)^2 \,\mathrm{d}\eta \approx 0.887\Omega^{-1/2} z^{1/2}, \tag{4.12}$$

where $W = Ra^{-1}w$, with w denoting the vertical component of $\boldsymbol{u}$. Here $\mathscr{C}$ appears only in a ratio with $\mathscr{S}$ (within $\Omega^{-1/2}$), so that increasing $\mathscr{C}$ serves to reduce the effective value of $\mathscr{S}$. The solid fraction locally decreases as $\mathscr{C}$ increases (provided Ra is fixed), and so more latent heat is required to be removed in order to achieve a given solutal flux. Perhaps surprisingly, smaller parameter values reverse the trend of variation with $\mathscr{C}$; this trend is, however, limited because the asymptotic results require both $\mathscr{S}$ and $\mathscr{C}$ to be large.

4.2. *Transient solution*

Here we are concerned with the manner in which the final equilibrium state, given by (4.7), is approached. Equation (3.3*b*) is hyperbolic in X and T and requires, in addition to the 'upstream' boundary condition (4.6), an initial condition on ϕ. We look for a transient self-similar solution of the form

$$\phi(X, z, T) = \bar{\phi}(\eta, \tau)/z^{1/2}, \quad \text{where} \quad \tau = \Omega^{1/2} T/z^{1/2}, \tag{4.13a, b}$$

and use the method of characteristics to obtain

$$\bar{\phi}(\eta, \tau) = \bar{\phi}_0(\eta + \tau) + \frac{1}{\Omega^{1/2}\bar{\mathscr{C}}} \left[\theta'(\eta) - \theta'(\eta + \tau)\right]. \tag{4.13c}$$

This solves the transient problem in terms of an initial condition $\phi_0(X, z) = \bar{\phi}_0(\eta)/z^{1/2}$. A particular form of the function $\bar{\phi}_0(\eta)$ depends on the history of the system over a time of $O(Ra^{-1})$ (see § 4.1). Nonetheless, we argue in favour of the initial state given by

$$\bar{\phi}_0(\eta) = \bar{\phi}_\infty = 0 \quad (\eta \geqslant 0), \quad \text{i.e.} \quad \phi_0(X, z) = 0 \quad (X \geqslant 0, z > 0). \tag{4.14a–c}$$

Our prescription (4.14*a*) rests on the idea that the transients in the thermal and flow fields evolve so quickly that they can preserve the solid fraction unchanged continually over the period of $O(Ra^{-1})$, i.e. in its far-field distribution defined by (4.6). Further, we take $\bar{\phi}_\infty = 0$ (see (4.14*b*)) so as to describe the evolution towards the steady state (4.7).

In (η, τ)-space, the transient solidification in the mushy region has the nature of a uniformly-propagating wave, the propagation velocity being given by the pulling speed. Of greater interest is a development of the compositional stratification in the eutectic solid which results from the temporal variation of the solid fraction at the eutectic boundary. Note that the dimensionless time T can also be interpreted as the dimensionless width of the eutectic solid formed. The bulk composition evolves from a uniform initial state $\Theta = -1$ and asymptotes to (4.10) as $T \to \infty$. At the interface the steady state is approached exponentially with a decay factor proportional to $\Omega^{-1/2} z^{1/2}$. The delay in the approach to steady state as height z increases gives rise to a compositional stratification in the solid typical of the long-time evolution of systems solidifying along a fixed vertical wall in large tanks (Huppert *et al.* 1987; cf. their figure 10).

5. Conclusion

A simple model of laterally solidifying mushy regions has been proposed which provides a clear physical description of the coupling between flow and solidification, and quantifies the associated fluxes of heat and solvent. Briefly, buoyancy due to the horizontal compositional drop across the mush drives convection confined to a thermal boundary layer along the eutectic front. Its width is determined by a balance among heat advection, cross-stream diffusion and latent-heat release, while the rate at which solute is carried by convection determines the local rate of solidification.

The analysis of this paper rests on the assumption that the permeability of the mush is uniform. Therefore, although the flow generally induces the local growth or dissolution of dendrites, the resulting alteration of the permeability and, in turn, self-adjustment of the convection pattern is not captured. A more detailed analysis, perhaps employing a non-similar solution technique, is required to incorporate this important nonlinear effect. Such an effect is expected to prevent the formation of a solid inclusion near the leading edge of the eutectic boundary.

The primary conclusion of this paper is that convection within the mush sets up significant solute stratification in the resulting solid product. Some of the available experimental data lend support to our results on solute macrosegregation. In typical experiments, however, convection is complicated for a variety of reasons, including the presence of a liquid region, double-diffusive instabilities and a finite container size. We hope that our idealized model will stimulate further theoretical investigations of this complex problem.

The authors are grateful to H. E. Huppert for his constructive comments on earlier versions of the manuscript. During the course of this work, P. G. was supported by the Royal Society under the Royal Society/NATO Postdoctoral Fellowship Programme.

Appendix. Approximate solution

A system equivalent to (3.3*a*), (3.3*c*), (2.4) and (2.5) can be written as

$$\Omega\left(U\frac{\partial\theta}{\partial X}-\theta\frac{\partial\theta}{\partial z}\right)=\frac{\partial^2\theta}{\partial X^2}, \tag{A 1a}$$

$$\frac{\partial U}{\partial X}-\frac{\partial\theta}{\partial z}=0, \tag{A 1b}$$

$$\theta=-1, \quad U=0 \quad \text{at} \quad X=0 \quad (z>0), \tag{A 2a,b}$$

$$\theta\to 0 \quad \text{as} \quad X\to\infty \quad (z>0\ ), \tag{A 2c}$$

where $U=Ra^{-1/2}u$ and u denotes the horizontal component of $\boldsymbol{u}$.

We construct an approximate solution to (A 1) and (A 2) by using a method of integral relations (Dorodnitsyn 1962). The method begins by the derivation of an integral relation that must be satisfied by the exact solution. On multiplying (A 1*b*) by a weighting function $p=p(\theta)$, possessing the property that it decays at least as fast as θ as $X\to\infty$, multiplying (A 1*a*) by $p'(\theta)$, adding the two and integrating across the boundary layer, we obtain

$$\frac{\mathrm{d}}{\mathrm{d}z}\int_{-1}^{0}\frac{1}{q(\theta)}p(\theta)\theta\,\mathrm{d}\theta=p'(-1)q_0(z)+\int_{-1}^{0}q(\theta)p''(\theta)\,\mathrm{d}\theta, \tag{A 3}$$

where θ has been used as independent variable instead of X by setting $q=\Omega^{-1/2}\partial\theta/\partial X$ and $q_0(z)\equiv q|_{\theta=-1}$.

A first approximation to the solution could be obtained by representing $q(\theta)$ by a first-order interpolating polynomial $q(\theta)=q_0(z)\theta$. Evaluating (A 3) with $p(\theta)=\theta$, we obtain $q_0=1/(2z)^{1/2}$ and $\theta=-\mathrm{e}^{-\eta/2}$, with η given by (4.1*c*). A more accurate approximation is obtained by using the second-order interpolating polynomials

$$q=2\theta\left[\left(\theta+\tfrac{1}{2}\right)q_0(z)-2(\theta+1)q_1(z)\right], \tag{A 4a}$$

$$1/q=\left[2\left(\theta+\tfrac{1}{2}\right)/q_0(z)-(\theta+1)/q_1(z)\right]/\theta, \tag{A 4b}$$

where $q_1(z)\equiv q|_{\theta=-1/2}$. Note that with these representations, (A 1) and (A 2) are satisfied at the boundaries of the two equally spaced intervals in θ-space, namely $\theta=-\frac{1}{2}$ and -1. To determine q_0 and q_1, (A 3) must be evaluated with two different weighting functions $p(\theta)$. We choose the linearly independent functions $p(\theta)=\theta$ and θ^2, and find that q_0 and q_1 satisfy

$$\frac{\mathrm{d}}{\mathrm{d}z}\left(\frac{1}{q_0}+\frac{1}{q_1}\right)=6q_0, \quad \frac{\mathrm{d}}{\mathrm{d}z}\left(\frac{2}{q_0}+\frac{1}{q_1}\right)=4(5q_0-4q_1), \tag{A 5a,b}$$

which are solved by

$$q_0=\bar{q}_0/z^{1/2}, \quad q_1=\bar{q}_1/z^{1/2}, \tag{A 6a,b}$$

with $1/\bar{q}_0^2=4(9-2\sqrt{15})$ and $1/\bar{q}_1^2=\frac{32}{7}(6-\sqrt{15})$. Equation (A 4*a*) can then be integrated to obtain

$$\theta=-b/[a+(b-a)\mathrm{e}^{b\eta}], \tag{A 7}$$

where $a = 2(2\bar{q}_1 - \bar{q}_0) \approx 0.390$ and $b = \bar{q}_0 - 4\bar{q}_1 \approx 0.836$. Equation (A 1$b$) gives, on integration and applying (A 2b),

$$U = -\frac{1}{2a}\frac{1}{\Omega^{1/2}}\frac{1}{z^{1/2}}\left[\ln\frac{b}{a+(b-a)\mathrm{e}^{b\eta}} + \frac{b(b-a)\eta\mathrm{e}^{b\eta}}{a+(b-a)\mathrm{e}^{b\eta}}\right]. \tag{A 8}$$

From (4.7) and (A 7), we find

$$\phi = b^2(b-a)\frac{1}{\Omega^{1/2}\mathscr{C}}\frac{1}{z^{1/2}}\frac{\mathrm{e}^{b\eta}}{[a+(b-a)\mathrm{e}^{b\eta}]^2}. \tag{A 9}$$

Finally, the flux of solvent, defined by (4.12), may, using (A 7), be expressed as

$$\mathscr{F}/Ra^{1/2} = \frac{1}{a}\left(\frac{b}{a}\ln\frac{b}{b-a} - 1\right)\frac{1}{\Omega^{1/2}}z^{1/2} \approx 0.889\Omega^{-1/2}z^{1/2}. \tag{A 10}$$

This Appendix provides approximate analytical solutions for key properties of the system.

REFERENCES

Bloomfield, L. J. & Huppert, H. E. 2003 Solidification and convection of a ternary solution cooled from the side. *J. Fluid Mech.* **489**, 269–299.

Cheng, P. & Minkowycz, W. J. 1977 Free convection about a vertical flat plate embedded in a porous medium with application to heat transfer from a dike. *J. Geophys. Res.* **82**, 2040–2044.

Dorodnitsyn, A. A. 1962 General method of integral relations and its application to boundary layer theory. In *Advances in Aeronautical Sciences* (ed. Th. von Kármán *et al.*), pp. 207–219. Pergamon.

Emms, P. W. & Fowler, A. C. 1994 Compositional convection in the solidification of binary alloys. *J. Fluid Mech.* **262**, 111–139.

Fearn, D. R. 1998 Hydromagnetic flow in planetary cores. *Rep. Prog. Phys.* **61**, 175–235.

Huppert, H. E. 1990 The fluid mechanics of solidification. *J. Fluid Mech.* **212**, 209–240.

Huppert, H. E. & Sparks, R. S. J. 1984 Double-diffusive convection due to crystallization in magmas. *Annu. Rev. Earth Planet. Sci.* **12**, 11–37.

Huppert, H. E., Sparks, R. S. J., Wilson, J. R., Hallworth, M. A. & Leitch, A. M. 1987 Laboratory experiments with aqueous solutions modelling magma chamber processes II. Cooling and crystallization along inclined planes. In *Origins of Igneous Layering* (ed. I. Parsons), pp. 539–568. Reidel.

Hurle, D. T. J. 1993 *Handbook of Crystal Growth*, vol. 1–3. North-Holland.

Ingham, D. B. & Brown, S. N. 1986 Flow past a suddenly heated vertical plate in a porous medium. *Proc. R. Soc. Lond.* A **403**, 51–80.

Kurz, W. & Fisher, D. J. 1989 *Fundamentals of Solidification.* Trans. Tech. Publications.

Leitch, A. M. 1987 Various aqueous solutions crystallizing from the side. In *Structure and Dynamics of Partially Solidified Systems* (ed. D. E. Loper), pp. 39–57. Martinus Nijhoff.

Nilson, R. H., McBirney, A. R. & Baker, B. H. 1985 Liquid fractionation. Part II: Fluid dynamics and quantitative implications for magmatic systems. *J. Volcanol. Geotherm. Res.* **24**, 25–54.

Thompson, M. E. & Szekely, J. 1988 Mathematical and physical modelling of double-diffusive convection of aqueous solutions crystallizing at a vertical wall. *J. Fluid. Mech.* **187**, 409–433.

Turner, J. S. & Gustafson, L. B. 1981 Fluid motions and compositional gradients produced by crystallization or melting at vertical boundaries. *J. Volcanol. Geotherm. Res.* **11**, 93–125.

Worster, M. G. 1997 Convection in mushy layers. *Annu. Rev. Fluid Mech.* **29**, 91–122.

Worster, M. G. 2000 Solidification of fluids. In *Perspectives in Fluid Dynamics: a Collective Introduction to Current Research* (ed. G. K. Batchelor, H. K. Moffatt & M. G. Worster), pp. 393–446. Cambridge University Press.